JACS
JOURNAL OF THE AMERICAN CHEMICAL SOCIETY
Article
pubs.acs.org/JACS

Fluxional σ-Bonds of the 2,5,8-Trimethylphenalenyl Dimer: Direct Observation of the Sixfold σ-Bond Shift via a π-Dimer

Kazuyuki Uchida,[†] Zhongyu Mou,[‡] Miklos Kertesz,*[,‡] and Takashi Kubo*[,†]

[†]Department of Chemistry, Graduate School of Science, Osaka University, Toyonaka, Osaka 560-0043, Japan
[‡]Department of Chemistry, Georgetown University, Washington, D.C. 20057, United States

Supporting Information

ABSTRACT: Direct evidence for σ-bond fluxionality in a phenalenyl σ-dimer was successfully obtained by a detailed investigation of the solution-state dynamics of 2,5,8-trimethylphenalenyl (TMPLY) using both experimental and theoretical approaches. TMPLY formed three diamagnetic dimers, namely, the σ-dimer (*RR*/*SS*), σ-dimer (*RS*), and π-dimer, which were fully characterized by ^{1}H NMR spectroscopy and electronic absorption measurements. The experimental findings gave the first quantitative insights into the essential preference of these competitive and unusual dimerization modes. The spectroscopic analyses suggested that the σ-dimer (*RR*/*SS*) is the most stable in terms of energy, whereas the others are metastable; the energy differences between these three isomers are less than 1 kcal mol^{-1}. Furthermore, the intriguing dynamics of the TMPLY dimers in the solution state were fully revealed by means of ^{1}H−^{1}H exchange spectroscopy (EXSY) measurements and variable-temperature ^{1}H NMR studies. Surprisingly, the σ-dimer (*RR*/*SS*) demonstrated a sixfold σ-bond shift between the six sets of α-carbon pairs. This unusual σ-bond fluxionality is ascribed to the presence of a direct interconversion pathway between the σ-dimer (*RR*/*SS*) and the π-dimer, which was unambiguously corroborated by the EXSY measurements. The proposed mechanism of the sixfold σ-bond shift based on the experimental findings was well-supported by theoretical calculations.

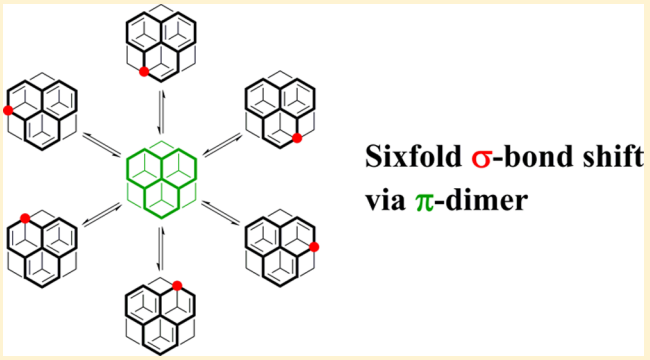

INTRODUCTION

Phenalenyl (**1**) is a neutral odd-alternant hydrocarbon radical that has a thermodynamically stabilized structure due to the extensive delocalization of its 13 π-electrons. The unpaired π-electron sits on a singly occupied molecular orbital (SOMO) that is delocalized over six α-carbon atoms.[1] Phenalenyls have attracted much interest from fundamental and materials chemists[2] because of the unique two-electron, 12-center (2e/12c) π-stacking bonding in its dimers and other aggregates, which is called "pancake bonding".[3−7] Over 100 derivatives have been synthesized, many of which display unusual properties.[2,7,8] Aggregation most often produces dimers, but chains have also been obtained in many cases, some with remarkably high conductivities[2] and others with complex magnetism.[9] Although σ-bond formation (2e/2c bonding) has been considered as a natural dimerization mode for hydrocarbon radicals,[10] the strong pancake bonding of phenalenyl, which is dominated by a covalent bonding interaction of the unpaired electrons in the SOMOs as well as van der Waals interactions,[5,11,12] leads to bimodal σ- and π-dimerization (Scheme 1).[13] Numerous efforts have been devoted to understanding the essential dimerization behavior of phenalenyls on the basis of experimental and theoretical approaches[14−19] after the first isolation of a pancake-bonded π-dimer of the phenalenyl derivative with three *tert*-butyl groups at the β positions (**2**).[20,21] Systematic studies of the dimerization modes of phenalenyl derivatives have suggested that the two dimerization channels are close in energy and that

Scheme 1. Dimerization Modes of Phenalenyl

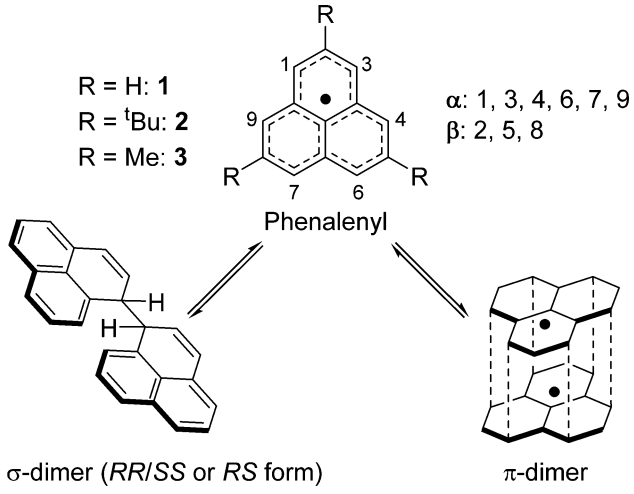

Received: February 18, 2016
Published: March 10, 2016

DOI: 10.1021/jacs.6b01791
J. Am. Chem. Soc. 2016, 138, 4665−4672

phenalenyl derivatives should demonstrate bimodal dimerization in solution and the solid state.[15,17,18] Indeed, 2,5,8-trimethylphenalenyl (TMPLY, **3**) was successfully isolated as both the σ- and π-dimers in crystalline form, which were fully characterized by X-ray crystallographic analysis.[18]

We present in this paper the direct observation of the σ-bond fluxionality demonstrated by the σ-dimer of the phenalenyl derivative TMPLY **3** in solution. We show that the highly symmetrical pancake-bonded π-dimer plays a key role as a highly stable intermediate in the unique σ-bond rearrangement reaction. We reveal, with strong evidence, that complex σ- and π-dimerization behaviors are present even in the solution state, as **3** actually forms three different diamagnetic dimers: the $\mathbf{3}_2$ σ-dimer (*RR*/*SS*), the $\mathbf{3}_2$ σ-dimer (*RS*), and the $\mathbf{3}_2$ π-dimer. Although these isomeric dimers interconvert, we were able to fully characterize them by a combination of ^{1}H NMR spectroscopy and electronic absorption measurements as well as computational studies. Whereas the σ- and π-dimerization modes were previously observed in the solid state,[18,22] the first observation of both modes in solution enabled us to elucidate quantitatively the relative preferences of the competing dimerization pathways. Moreover, the $\mathbf{3}_2$ σ-dimer (*RR*/*SS*) demonstrates a sixfold σ-bond shift, which was unambiguously confirmed by ^{1}H−^{1}H exchange spectroscopy (EXSY) measurements, that could be described as a constant spinning and tilting of a pair of plates representing the phenalenyl moiety. The continuous transformation of the chemical bonding motif from a σ-bond to a pancake bond plays an important role in the mechanism of the unique σ-bond migration. The presence of a direct interconversion process between the $\mathbf{3}_2$ σ-dimer (*RR*/*SS*) and the $\mathbf{3}_2$ π-dimer was corroborated experimentally, suggesting that the sixfold σ-bond shift takes place via the $\mathbf{3}_2$ π-dimer as an intermediate. We also present computational evidence for the complex isomerization of the dimers, fully supporting the experiment-based mechanism of the fluxional interconversion of the σ- and π-bonded dimeric aggregates.

RESULTS

Dimerization Modes of 2,5,8-Trimethylphenalenyl (3) in the Solution State. The formation of diamagnetic dimers ($\mathbf{3}_2$) was confirmed by variable-temperature (VT) electron spin resonance (ESR) measurements. The ESR signal corresponding to monomeric **3** recorded in degassed tetrahydrofuran (THF) decreased in intensity with decreasing temperature and disappeared completely at 170 K (Figure 1), suggesting the formation of dimer species ($\mathbf{3}_2$), similar to the case of $\mathbf{2}_2$.[13] By means of a van't Hoff plot (Figure S1b in the Supporting Information), the thermodynamic parameters for dimerization were estimated as $\Delta H = -9.4 \pm 0.19$ kcal mol^{-1} and $\Delta S = -22 \pm 0.92$ cal K^{-1} mol^{-1}, which are nearly identical to those determined in toluene.[18] However, the formation of dimers at low temperature leaves open the question as to the bonding characteristics of these dimers.

The dimerization modes of **3** in solution were revealed by ^{1}H NMR spectroscopy. The ^{1}H NMR spectrum of **3** recorded in degassed THF-d_8 at 173 K is shown in Figure 2. **3** presents a complicated ^{1}H NMR spectrum arising from three diamagnetic dimer species, which were unambiguously characterized as the $\mathbf{3}_2$ σ-dimer (*RR*/*SS*), the $\mathbf{3}_2$ σ-dimer (*RS*), and the $\mathbf{3}_2$ π-dimer on the basis of two-dimensional NMR techniques as well as theoretical predictions of NMR chemical shifts calculated using density functional theory (DFT) at the GIAO-(U)B3LYP/6-31+G(d,p) level (Figures S2−S4 and Table S1). The $\mathbf{3}_2$ σ-dimer (*RR*/*SS*) with C_2 symmetry shows six prominent singlets in the 8−4 ppm region corresponding to protons on the phenalenyl moieties and three singlets in the 3−1 ppm region for the methyl protons. In contrast to the spectral simplicity of the $\mathbf{3}_2$ σ-dimer (*RR*/*SS*) with C_2 symmetry, the $\mathbf{3}_2$ σ-dimer (*RS*) has C_1 symmetry. This low-symmetry structure affords 12 singlet peaks in the 8−4 ppm region corresponding to the two independent phenalenyl moieties. It should be noted that a singlet peak corresponding to one of the aromatic protons, H_b, is shifted upfield to 5.46 ppm as a result of the strong shielding effect arising from the ring current of the neighboring phenalenyl ring (Table S1). This result is consistent with the computational prediction in which H_b is in the vicinity of the other phenalenyl plane. Moreover, characteristic broadened signals at 6.5 and 2.2 ppm are assignable to the $\mathbf{3}_2$ π-dimer. The chemical shift of the broad peak corresponding to the α-protons on the phenalenyl moiety is almost identical to those of the triphenyl derivative (6.8 ppm)[18] and the tri-*tert*-butyl derivative **2** (6.5 ppm).[3]

The ratio of the integrated ^{1}H NMR signals gives the first quantitative insight into the preferred dimerization mode. The $\mathbf{3}_2$ σ-dimer (*RR*/*SS*), which shows the most intense NMR signals, is energetically the most favorable isomer. Although the $\mathbf{3}_2$ σ-dimer (*RS*) is 0.08 kcal mol^{-1} less stable in energy than the $\mathbf{3}_2$ σ-dimer (*RR*/*SS*) on the basis of the ratio of the NMR signal

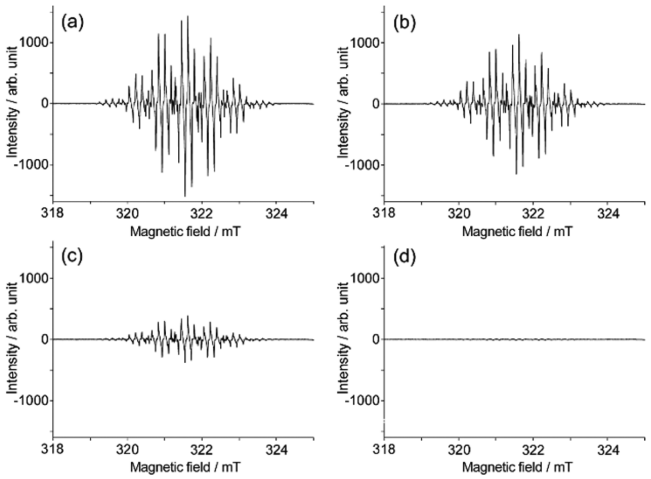

Figure 1. ESR spectra of **3** measured in degassed THF at (a) 280 K, (b) 250 K, (c) 220 K, and (d) 170 K.

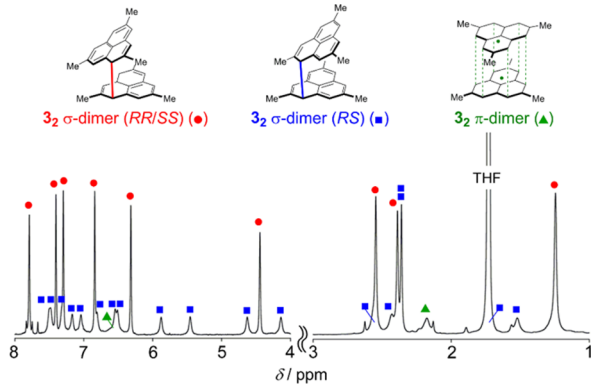

Figure 2. ^{1}H NMR spectrum of $\mathbf{3}_2$ dimers measured in degassed THF-d_8 at 173 K. The aromatic and olefinic region (8−4 ppm) is magnified 3 times relative to the aliphatic region (3−1 ppm) for ease of visualization.

DOI: 10.1021/jacs.6b01791
J. Am. Chem. Soc. 2016, 138, 4665−4672

intensities and the Boltzmann distribution, the energy difference is extraordinarily small. In comparison with the 3_2 σ-dimer (*RR*/*SS*), the 3_2 π-dimer, which shows the weakest NMR signals among the three dimers, is 0.68 kcal mol^{-1} less stable in energy. This quantitative estimation of the preference among the dimerization modes suggests that σ-dimerization is energetically more favorable, although the energy difference between the σ- and π-dimers is extremely small, which is well-consistent with the theoretical prediction that the σ- and π-dimerization pathways of phenalenyl are energetically competitive and depend on the substituents.[13,18] The experimentally determined energetic preference of 3_2 is consistent with the computational results in that the 3_2 σ-dimer (*RS*) and the 3_2 π-dimer are 1.21 and 3.64 kcal mol^{-1} less stable in energy than the 3_2 σ-dimer (*RR*/*SS*), respectively (these values include zero-point energy (ZPE) corrections).

The formation of the metastable 3_2 π-dimer in solution was confirmed by a VT electronic absorption measurement within the temperature range from 295 to 173 K. A dilute solution of **3** showed a weak and sharp absorption band (550 nm, ε = 320 cm^{-1} M^{-1}) at room temperature (Figure S5), which corresponds to a forbidden transition of monomeric **3** based on the absorption spectrum of monomeric **2**, also measured in dilute solution.[14,20] Gradual cooling of **3** in THF resulted in the appearance of a broad absorption band at 500 to 600 nm (Figure 3a). Whereas the σ-dimers of the phenalenyl derivatives

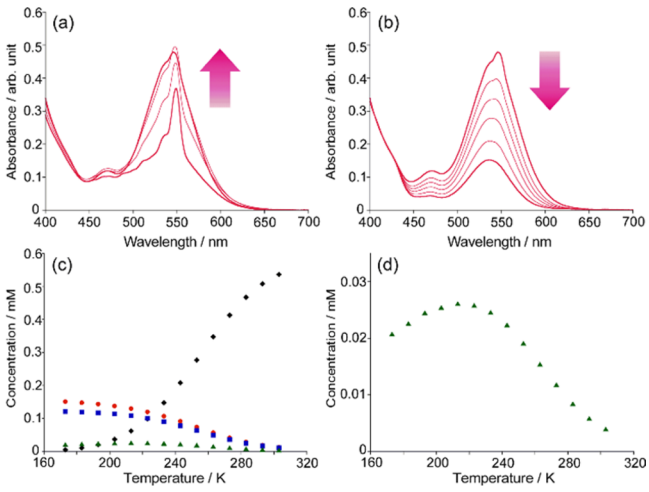

Figure 3. (a, b) VT electronic absorption spectra of **3** (5.9 × 10^{-4} M) in degassed THF measured over the temperature range (a) from 295 to 233 K and (b) from 233 to 173 K. (c) Simulated concentrations of monomeric **3** and its dimers 3_2 at each temperature, assuming a 5.9 × 10^{-4} M solution of **3**. The concentrations of monomeric **3**, 3_2 σ-dimer (*RR*/*SS*), 3_2 σ-dimer (*RS*), and 3_2 π-dimer are shown as black ◆, red ●, blue ■, and green ▲, respectively. (d) Magnified view of the simulated concentration of the 3_2 π-dimer (green ▲).

show no characteristic absorption band in the visible region, the π-dimers of the phenalenyl derivatives are known to show a broad and intense absorption band near 500 to 600 nm arising from their HOMO−LUMO transitions.[15,16] Thus, the successive growth of the broad absorption band in the visible region can be ascribed to an increase in the concentration of the 3_2 π-dimer. Interestingly, unlike the spectral change observed in the VT electronic absorption measurements of **2**,[14] the absorption spectrum of **3** showed a peculiar temperature dependence as the temperature was decreased from 233 to 173 K. Cooling over this range resulted in a decrease in the intensity of the absorption band corresponding to the 3_2 π-dimer (Figure 3b). To understand this characteristic behavior, the concentrations of monomeric **3** and its dimers (3_2 σ-dimer (*RR*/*SS*), 3_2 σ-dimer (*RS*), and 3_2 π-dimer) were simulated using the thermodynamic parameters for dimerization, which were determined by VT ESR measurements, and the energy differences between the 3_2 dimers, which were obtained by ^{1}H NMR spectroscopy (see Figure 3c). The concentration of monomeric **3** decreases with decreasing temperature, whereas the concentrations of the diamagnetic dimers increase as a result of the thermodynamic equilibrium. Notably, the population ratio among the different 3_2 dimers follows the Boltzmann distribution, suggesting that the ratios of the populations of the metastable 3_2 σ-dimer (*RS*) and 3_2 π-dimer to the population of the 3_2 σ-dimer (*RR*/*SS*) should decrease with decreasing temperature. The simulated concentration plot for the 3_2 π-dimer in Figure 3d predicts that its concentration should reach a maximum at 213−223 K. Indeed, the intensity of the absorption band of the 3_2 π-dimer reached a maximum value at 233 K, which is very consistent with the concentration simulation. Hence, the characteristic behavior observed in the VT electronic absorption measurements strongly corroborates the quantitative results obtained by ^{1}H NMR spectroscopy, which showed that the 3_2 π-dimer is a metastable species.

In the VT electronic absorption measurements on **3**, the broad absorption band centered at 536 nm was still present even at 173 K. Because the concentration of monomeric **3** is estimated to be 5 × 10^{-6} M on the basis of the concentration simulation shown in Figure 3c, the absorption due to monomeric **3** is negligible. Thus, the absorption band observed at 173 K is assignable to the intrinsic HOMO−LUMO transition of the 3_2 π-dimer. The HOMO and LUMO of the π-dimer of phenalenyl arise from the bonding and antibonding combinations of the SOMOs; therefore, the HOMO−LUMO transition of the π-dimer significantly reflects the nature of pancake bonding.[18] The absorption band of the 3_2 π-dimer shows a blue shift with respect to that of the 2_2 π-dimer (λ_{max} = 595 nm).[14] This result suggests that the covalent bonding interaction between the two phenalenyl moieties in the 3_2 π-dimer is more effective than that in the 2_2 π-dimer. It is reasonable to attribute this difference to the replacement of the bulky *tert*-butyl groups with the sterically less hindered methyl groups. This spectroscopic result is fully supported by the molecular geometries determined by the X-ray crystallographic analysis and computational studies. The 3_2 π-dimer has shorter C_α−C_α distances (X-ray, 3.054 Å on average at 100 K; UM05-2X calculation, 2.950 Å) compared with the 2_2 π-dimer (X-ray, 3.306 Å at 300 K; UM05-2X calculation, 3.298 Å) because of stronger pancake bonding.[18,20]

Solution-State Dynamics of TMPLY Dimers (3_2). To shed light on the dynamics of 3_2 in solution, EXSY measurements were performed in degassed THF-d_8 at 173 K (Figure 4). First, we focused on the dynamics of the 3_2 σ-dimer (*RS*). This dimer shows cross-peaks with the same signs as the diagonal peaks (Figure 4a) due to the mutual site exchange of protons in each α-proton pair (i.e., H_a/H'_a, H_b/H'_b, etc.), which is caused by the conformational change between the stable conformations with C_1 symmetry (*RS*1 and *RS*3 in Scheme 2). At higher temperature, the nonequivalent signals for each α-proton pair coalesce into an averaged signal because of the

DOI: 10.1021/jacs.6b01791
J. Am. Chem. Soc. 2016, 138, 4665−4672

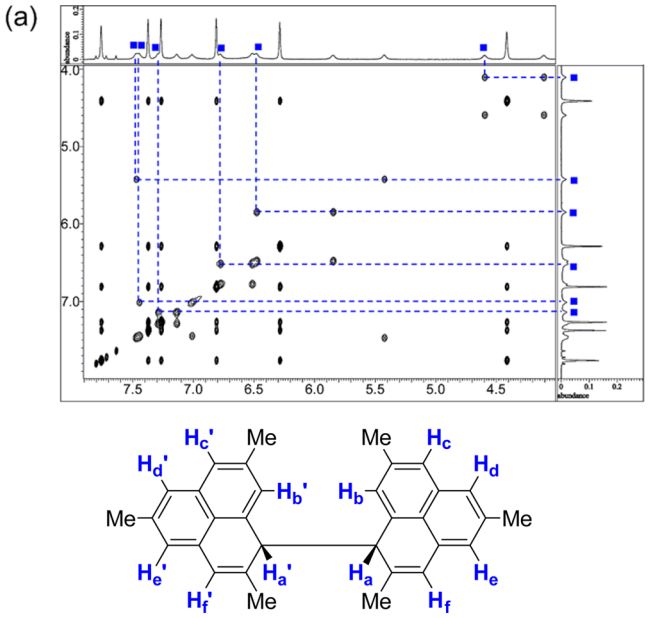

Figure 4. ^{1}H−^{1}H EXSY spectrum of $\mathbf{3}_2$ dimers in the range of 8−4 ppm, measured in THF-d_8 at 173 K (mixing time = 500 ms). (a) Cross-correlations between protons of the $\mathbf{3}_2$ σ-dimer (*RS*) are depicted with blue lines, and (b) cross-correlations between protons of the $\mathbf{3}_2$ σ-dimer (*RR*/*SS*) are depicted with red lines.

Scheme 2. Conformational Change between Stable Conformations with C_1 Symmetry (*RS*1 and *RS*3 Enantiomers; see Figure 6)[a]

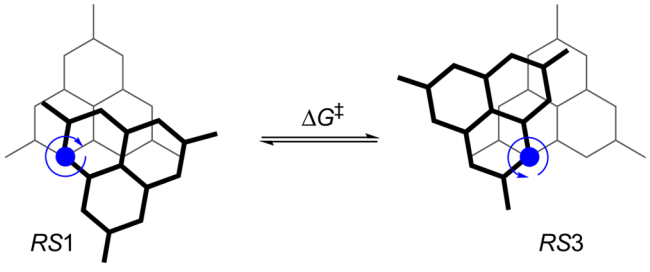

[a]The position of the C(sp^3)−C(sp^3) σ-bond is indicated by a blue dot.

rapid interconversion between *RS*1 and *RS*3, as shown in Figure 5a.

The activation free energy ($\Delta G^{\ddagger}$) for the conformational change can be estimated from the exchange rate (k_{ex}) and the

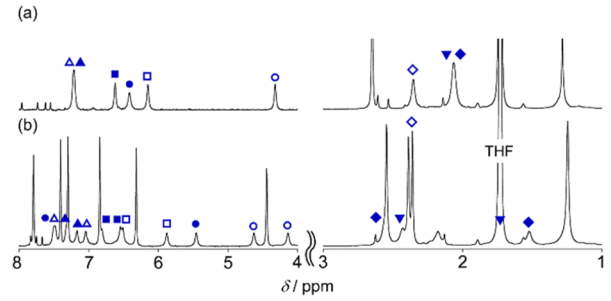

Figure 5. VT ^{1}H NMR spectra of $\mathbf{3}_2$ dimers recorded at (a) 263 K and (b) 173 K. Corresponding peaks of α-proton pairs are indicated with the same symbols.

coalescence temperature (T_c) of an exchanging pair of signals. Focusing on the signals corresponding to benzyl protons observed at 4.14 and 4.63 ppm as representative, the exchange rate k_{ex} at the coalescence temperature (T_c = 191 K; Figure S7) was determined to be 435 s^{-1} via the equation $k_{ex} = \pi\Delta\nu/\sqrt{2}$, where $\Delta\nu$ is the frequency separation of the two corresponding peaks ($\Delta\nu$ = 196 Hz for the pair of benzyl protons H_a). Therefore, the activation free energy for the conformational change between *RS*1 and *RS*3 was determined from the Eyring equation to be 8.7 kcal mol^{-1}. This experimental estimation was fully supported by the relaxed torsional energy scan along the central σ-bond calculated at the M05-2X/6-31G(d,p) level (Figure 6). The rotational scan represents a symmetrical

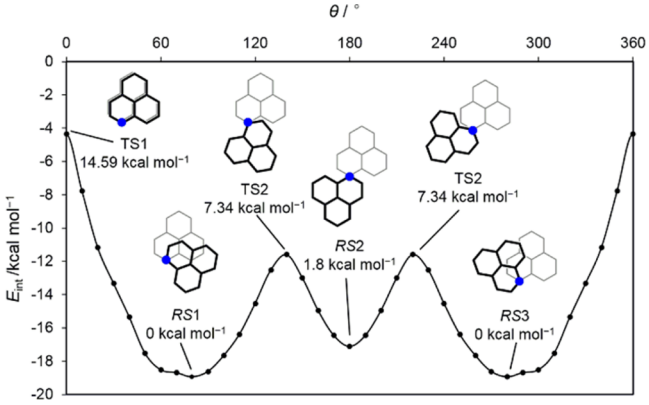

Figure 6. Relaxed torsional energy scan of the $\mathbf{3}_2$ σ-dimer (*RS*) as a function of the angle θ for rotation around the σ-bond of the $\mathbf{3}_2$ σ-dimer (*RS*). Energies were calculated at the M05-2X/6-31G(d,p) level. The position of the C(sp^3)−C(sp^3) σ-bond is indicated with a blue dot.

potential energy surface with three local minima (*RS*1, *RS*2, and *RS*3) and the corresponding transition structures (TS1 and TS2). The symmetry can be expressed as

$$E(\theta) = E(-\theta) = E(360^\circ - \theta) \quad (1)$$

since *RS*1 and *RS*3 are enantiomers. The conformational change between *RS*1 and *RS*3 takes place through TS2; thus, the activation barrier is estimated to be 7.34 kcal mol^{-1} (without ZPE corrections), which is comparable to the activation free energy determined experimentally.

In contrast to the simplicity of the ^{1}H−^{1}H EXSY cross-peaks arising from the $\mathbf{3}_2$ σ-dimer (*RS*), the structural isomer, the $\mathbf{3}_2$ σ-dimer (*RR*/*SS*), showed a unique feature in its EXSY measurements; that is, each α-proton showed cross-peaks with

DOI: 10.1021/jacs.6b01791
J. Am. Chem. Soc. 2016, 138, 4665−4672

all of the remaining α-protons due to chemical exchange (see Figure 4b). This intriguing phenomenon can be ascribed to a sixfold σ-bond shift among the six sets of α-carbon pairs (i.e., C_{a1}/C_{a2}, C_{b1}/C_{f2}, C_{c1}/C_{e2}, C_{d1}/C_{d2}, C_{e1}/C_{c2}, and C_{f1}/C_{b2}) within the time scale of the EXSY measurement, as illustrated in Scheme 3. To obtain a deeper understanding of the

Scheme 3. σ-Bond Shift in the 3_2 σ-Dimer (*RR*/*SS*)[a]

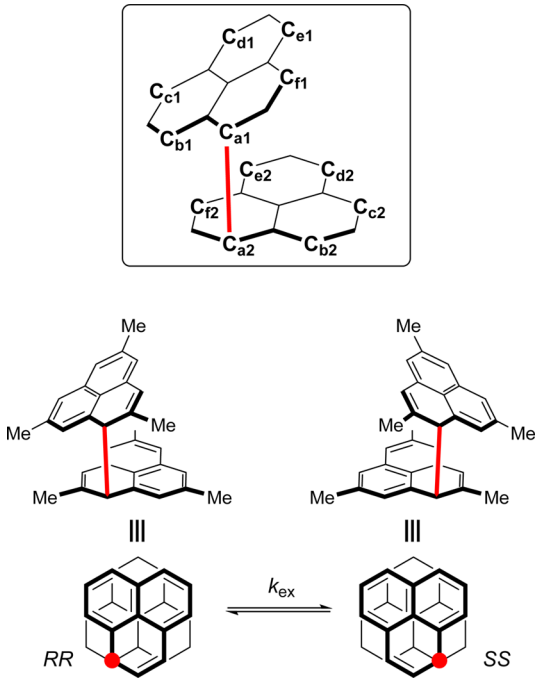

[a]Only the shifts between the C_{a1}/C_{a2} and C_{f1}/C_{b2} pairs are shown, and the position of the $C(sp^3)$–$C(sp^3)$ σ-bond is shown with a red dot.

mechanism of the sixfold σ-bond shift, the exchange rates (k_{ex}) were estimated from the mixing-time dependence of the intensities of the diagonal peaks and cross-peaks arising from the corresponding pairs of signals (Figure S8).[23] The dynamic processes taking place between H_a and H_c–H_f gave almost the same exchange rates at 173 K (k_{ex} = 0.7–0.8 s^{-1}), whereas the exchange rate between H_a and H_b was slightly larger (k_{ex} = 2 s^{-1}). It should be noted that the cross-peaks between H_a and H_b, which are in close proximity to each other, include a non-negligible contribution from a dipole–dipole interaction (nuclear Overhauser effect); thus, the exchange rate between H_a and H_b determined from the intensity ratio of the EXSY peaks would not reflect the kinetics of the σ-bond shift.

Focusing on the aliphatic region of the ^1H–^1H EXSY spectrum shown in Figure 7, explicit cross-peaks between the methyl protons of the 3_2 σ-dimer (*RR*/*SS*) and those of the 3_2 π-dimer can be found, which provides direct evidence for the presence of a dynamic equilibrium between these two species. It should be noted that no cross-peaks between the 3_2 σ-dimer (*RS*) and the 3_2 π-dimer are observed. As illustrated in Scheme 4, the dynamic exchange between the σ-dimer (*RR*/*SS*) and the staggered π-dimer starts with a rotation about the $C(sp^3)$–$C(sp^3)$ σ-bond and the simultaneous elongation of that σ-bond. On the other hand, the σ-dimer (*RS*) cannot be converted into the π-dimer without dissociation into monomeric radicals because, as shown in Scheme 2, rotation around the $C(sp^3)$–$C(sp^3)$ σ-bond in the σ-dimer (*RS*) results in the eclipsed overlap of the molecular skeleton, and the corresponding π-

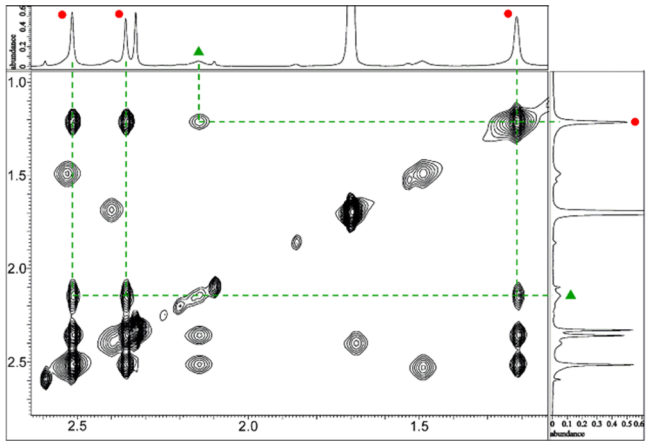

Figure 7. Aliphatic region (3–1 ppm) of the ^1H–^1H EXSY spectrum of the 3_2 dimers measured in THF-d_8 at 173 K (mixing time = 500 ms). Cross-correlations between the protons of the 3_2 σ-dimer (*RR*/*SS*) and the 3_2 π-dimer are depicted with green lines.

Scheme 4. Dynamic Exchange between the 3_2 Dimers[a]

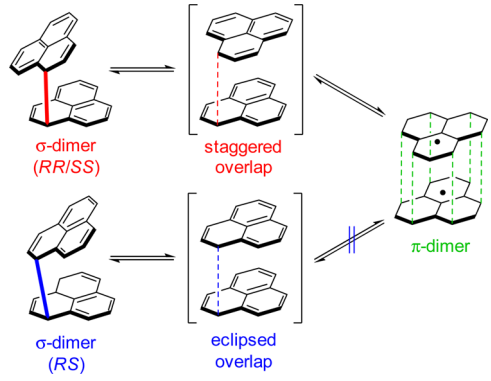

[a]Methyl groups have been omitted for clarity.

dimer is destabilized.[5] Thus, the EXSY results strictly preclude the possibility that the dynamic exchange between the 3_2 σ-dimer (*RR*/*SS*) and the 3_2 π-dimer proceeds via monomeric **3** radicals generated by the dissociation of these dimers.

DISCUSSION

The detailed investigation of the solution-state dynamics of the neutral radical **3** has provided insight into the fluxional σ-bond of the phenalenyl dimer. The 3_2 σ-dimer (*RR*/*SS*) showed a sixfold σ-bond shift within the time scale of the ^1H–^1H EXSY measurements. On the basis of these experimental results, two reaction mechanisms are possible: (1) a concerted [*m*,*m*]-sigmatropic rearrangement (Scheme 5a), and (2) a stepwise isomerization via the 3_2 π-dimer as an intermediate (Scheme 5b).

In general, the exchange rate of the σ-bond shift depends significantly on the molecular geometry. It is known that the $C(sp^3)$–B σ-bond shift of 1-phenalenyl(dipropyl)borane, which was fully investigated by ^1H–^1H EXSY measurements, takes place between spatially close α-carbon atoms ([1,3]-sigmatropic rearrangement).[24] Analogous fluxional bonding has been observed in organometallic chemistry[25] and main-group inorganic chemistry.[26] Although two dynamic processes, $[1,3]^9$-B and $[1,3]^3$-B migrations, were confirmed from the EXSY measurements, a significant difference in the exchange

DOI: 10.1021/jacs.6b01791
J. Am. Chem. Soc. 2016, 138, 4665–4672

Scheme 5. Proposed Mechanisms for the Sixfold σ-Bond Shift: (a) Concerted [*m*,*m*]-Sigmatropic Rearrangements within the 3_2 σ-Dimer (*RR*/*SS*); (b) Stepwise σ-Bond Shifts via the 3_2 π-Dimer as an Intermediate[a]

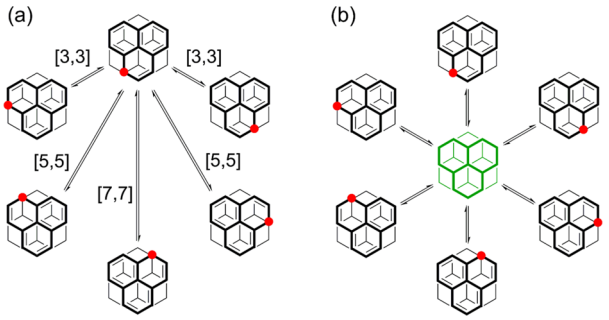

[a]The position of the C(sp^3)−C(sp^3) σ-bond is shown with a red dot.

rates due to the difference in the molecular topology was observed. Here we focused on the molecular geometry of the 3_2 σ-dimer (*RR*/*SS*) based on the X-ray crystallographic data in order to understand the mechanism of the sixfold σ-bond shift. The distances between the carbon atoms in each α-carbon pair are summarized in Table 1. The C_{d1}−C_{d2} distance of 6.298 Å is considerably longer than the C_{b1}−C_{f2} distance of 3.355 Å, inferring the presence of a noticeable difference in the exchange rates for [3,3]- and [7,7]-sigmatropic rearrangements. However, in fact, no significant difference in the exchange rates was observed (Figure S8). This finding strongly suggests that the sixfold σ-bond shift takes place in equal probabilities among the six sets of α-carbon pairs. The nonselective σ-bond shift is explained by a stepwise mechanism via the 3_2 π-dimer. The stepwise reaction is anticipated to proceed through dynamic exchange between the 3_2 σ-dimer (*RR*/*SS*) and the 3_2 π-dimer along with recurrent σ-bond dissociation−re-formation in the six sets of α-carbon pairs. The σ-bond re-formation in the 3_2 π-dimer with D_{3d} symmetry should take place in equal probabilities between the six structurally identical sets of α-carbon pairs. The interconversion between the 3_2 σ-dimer (*RR*/*SS*) and the 3_2 π-dimer was indeed corroborated experimentally by EXSY measurements; thus, the unique σ-bond shift demonstrated by the 3_2 σ-dimer (*RR*/*SS*) is expected to proceed in a stepwise mechanism via the 3_2 π-dimer as an intermediate.

Table 1. Distances between the Carbon Atoms in Each α-Carbon Pair of the 3_2 σ-Dimer (*RR*/*SS*) As Determined by X-ray Crystallographic Analysis and M05-2X Calculations[18]

	distance/Å	
α-carbon pair	X-ray	M05-2X
C_{a1}−C_{a2}	1.614	1.607
C_{b1}−C_{f2}	3.355	3.255
C_{c1}−C_{e2}	5.132	4.422
C_{d1}−C_{d2}	6.298	5.001
C_{e1}−C_{c2}	5.591	4.422
C_{f1}−C_{b2}	3.582	3.255

These experimental findings are supported by theoretical calculations. In our DFT calculations, the isomerization route between the 3_2 σ-dimer (*RR*/*SS*) and the 3_2 π-dimer was well elucidated, and the TS was successfully located. The potential energy surface (PES) of this isomerization is illustrated in Figure 15 of ref 18. Those calculations showed a σ- to π-isomerization barrier of only 7.14 kcal mol^{-1}. This rather small barrier is in good agreement with the experimental findings in this study, which allowed us to conclude that the 3_2 σ-dimer (*RR*/*SS*) and the 3_2 π-dimer coexist and interconvert rapidly in solution. Furthermore, we tried to determine the pathway for the [3,3]-sigmatropic rearrangement for the 3_2 σ-dimer (*RR*/*SS*). However, the TS we found for such a sigmatropic rearrangement was exactly the same one as in the σ- to π-isomerization process discussed in ref 18. This finding suggests that the σ-bond shifting between the 3_2 *RR*/*SS* σ-dimers proceeds through the 3_2 π-dimer as a stable intermediate. In other words, if the 3_2 π-dimer were unstable, the [3,3]-sigmatropic rearrangement might have occurred, and the corresponding TS might have been different from the TS in the σ- to π-isomerization process. Therefore, our calculations reinforced the experimental data that the σ-bond shift between the 3_2 σ-dimers (*RR*/*SS*) occurs through the stable 3_2 π-dimer intermediate. It also explains why the exchange rates are not different for the [3,3]- and [7,7]-sigmatropic rearrangements in the present case.

CONCLUSION

We have presented the bimodal dimerization of 2,5,8-trimethylphenalenyl (TMPLY, **3**) and the first observation of σ-bond fluxionality demonstrated by the 3_2 dimers in the solution state. **3** forms three diamagnetic dimers, namely, the 3_2 σ-dimer (*RR*/*SS*), 3_2 σ-dimer (*RS*), and 3_2 π-dimer, which were fully characterized by spectroscopic analyses as well as computational studies. The energetic preference among the dimerization modes was undoubtedly confirmed by ^{1}H NMR spectroscopy, which indicated that the 3_2 σ-dimer (*RR*/*SS*) is the most stable configuration and that the others are metastable dimers. As predicted by computational studies, the energy differences among the three dimers are extraordinarily small (less than 1 kcal mol^{-1}). Furthermore, a detailed investigation of the solution-state dynamics of the 3_2 dimers gave direct evidence for the σ-bond fluxionality of the phenalenyl σ-dimer. The 3_2 σ-dimer (*RR*/*SS*) demonstrates a sixfold σ-bond shift that takes place between six sets of α-carbon pairs with equal probabilities. This unique reaction is ascribed to a dynamic exchange between the 3_2 σ-dimer (*RR*/*SS*) and 3_2 π-dimer, which was corroborated experimentally by ^{1}H−^{1}H EXSY measurements. The interconversion between the 3_2 σ-dimer (*RR*/*SS*) and 3_2 π-dimer results in continuous σ-bond dissociation and re-formation among the six sets of α-carbon pairs, leading to the random σ-bond shifts.

METHODS

Experimental Methods. TMPLY **3** was prepared according to the synthetic procedure reported previously.[18] Anhydrous dichloromethane and THF were purchased from Kanto Chemical Co., Inc. and used without further purification. THF-d_8 for ^{1}H NMR and EXSY measurements was dried over Na−K alloy and distilled under reduced pressure. All of the spectroscopic measurements on **3** were conducted in solvents degassed by a repeated freeze−pump−thaw technique (four times). ESR spectra were recorded in THF on a JEOL JES-RE1X spectrometer over the temperature range from 300 to 170 K. ^{1}H NMR spectra and ^{1}H−^{1}H EXSY measurements were performed on a JEOL ECS400 spectrometer. The electronic absorption spectra in dichloromethane and THF were measured on JASCO V-570 and Shimadzu UV-3100PC spectrometers, respectively.

Computational Details. We employed M05-2X, a meta-generalized gradient approximation (mGGA) density functional for

DOI: 10.1021/jacs.6b01791
J. Am. Chem. Soc. 2016, 138, 4665−4672

geometry optimizations and energy calculations.[27] We also adopted B3LYP, a hybrid functional, for NMR calculations with the GIAO-(U)B3LYP/6-31+G(d,p) method.[28] For open-shell species such as monomer radicals and π-dimers, the broken-symmetry spin-unrestricted method was adopted (denoted with the prefix (U)). No broken-symmetry treatment was used for the closed-shell species such as the *RR*/*SS* and *RS* σ-dimers. The 6-31+G(d,p) basis set was used for NMR calculations, while 6-31G(d,p) basis set was used for geometry optimizations and energy calculations. The interaction energy (E_{int}) was calculated by the taking the difference of the total energies of the dimer and its monomers:

$$E_{int} = E_{tot}(\text{dimer}) - 2E_{tot}(\text{monomer}) \quad (2)$$

The details of bond-rotation scans in σ-dimers and bond-stretching studies between σ-dimers and π-dimers can be found in our previous study.[18] Vibrational frequency calculations were performed on stationary points to ensure the characteristics of minima (no imaginary frequency) and TSs (one imaginary frequency). ZPE corrections were applied to the minima and TSs but not applied for scans. All of the quantum-mechanical calculations were performed with the Gaussian 09 package (revision D.01).[29]

■ ASSOCIATED CONTENT

Supporting Information

The Supporting Information is available free of charge on the ACS Publications website at DOI: 10.1021/jacs.6b01791.

Experimental and computational details and Cartesian coordinates (PDF)

■ AUTHOR INFORMATION

Corresponding Authors

*kertesz@georgetown.edu

*kubo@chem.sci.osaka-u.ac.jp

Notes

The authors declare no competing financial interest.

■ ACKNOWLEDGMENTS

This article is dedicated to Professor Ichiro Murata on the occasion of his 88th birthday (Beiju). K.U. acknowledges support from a JSPS Fellowship for Young Scientists (2615260). T.K. thanks JSPS for a KAKENHI Grant (26288016) and MEXT for a Grant-in-Aid for Scientific Research on Innovative Areas "Photosynergetics" (Grant 15H01086). We thank the U.S. National Science Foundation for its support of this research at Georgetown University (Grant CHE-1006702). M.K. is member of the Georgetown Institute of Soft Matter. We also thank Dr. S. Tojo and Prof. T. Majima (The Institute of Scientific and Industrial Research (SANKEN), Osaka University) for their kind help with the VT electronic absorption measurements.

■ REFERENCES

(1) (a) Reid, D. H. *Tetrahedron* **1958**, *3*, 339. (b) Gerson, F. *Helv. Chim. Acta* **1966**, *49*, 1463. (c) Reid, D. H. *Chem. Ind.* **1956**, 1504. (d) Sogo, P. B.; Nakazaki, M.; Calvin, M. *J. Chem. Phys.* **1957**, *26*, 1343. (e) Paskovich, D. H.; Reddoch, A. H. *J. Am. Chem. Soc.* **1972**, *94*, 6938. In phenalenyl derivatives, the 1-, 3-, 4-, 6-, 7-, and 9-positions are called the α positions and the 2-, 5-, and 8-positions are called the β positions.

(2) For example, see: (a) Haddon, R. C. *ChemPhysChem* **2012**, *13*, 3581. (b) Pal, S. K.; Itkis, M. E.; Tham, F. S.; Reed, R. W.; Oakley, R. T.; Haddon, R. C. *Science* **2005**, *309*, 281. (c) Bag, P.; Itkis, M. E.; Stekovic, D.; Pal, S. K.; Tham, F. S.; Haddon, R. C. *J. Am. Chem. Soc.* **2015**, *137*, 10000.

(3) Suzuki, S.; Morita, Y.; Fukui, K.; Sato, K.; Shiomi, D.; Takui, T.; Nakasuji, K. *J. Am. Chem. Soc.* **2006**, *128*, 2530.

(4) Tian, Y.-H.; Kertesz, M. *J. Am. Chem. Soc.* **2010**, *132*, 10648.

(5) Cui, Z. H.; Lischka, H.; Beneberu, H. Z.; Kertesz, M. *J. Am. Chem. Soc.* **2014**, *136*, 5539.

(6) Yoneda, K.; Nakano, M.; Fukuda, K.; Matsui, H.; Takamuku, S.; Hirosaki, Y.; Kubo, T.; Kamada, K.; Champagne, B. *Chem. - Eur. J.* **2014**, *20*, 11129.

(7) (a) Cui, Z. H.; Gupta, A.; Lischka, H.; Kertesz, M. *Phys. Chem. Chem. Phys.* **2015**, *17*, 23963. (b) Kolb, B.; Kertesz, M.; Thonhauser, T. *J. Phys. Chem. A* **2013**, *117*, 3642.

(8) For recent reviews, see: (a) Preuss, K. *Polyhedron* **2014**, *79*, 1. (b) Kubo, T. *Chem. Rec.* **2015**, *15*, 218.

(9) (a) Kubo, T.; Shimizu, A.; Sakamoto, M.; Uruichi, M.; Yakushi, K.; Nakano, M.; Shiomi, D.; Sato, K.; Takui, T.; Morita, Y.; Nakasuji, K. *Angew. Chem., Int. Ed.* **2005**, *44*, 6564. (b) Huang, J.; Kertesz, M. *J. Am. Chem. Soc.* **2007**, *129*, 1634.

(10) Fossey, J.; Lefort, D.; Sorba, J. *Free Radicals in Organic Chemistry*; John Wiley & Sons: Chichester, U.K., 1995.

(11) Mota, F.; Miller, J. S.; Novoa, J. J. *J. Am. Chem. Soc.* **2009**, *131*, 7699.

(12) Tian, Y.-H.; Huang, J.; Kertesz, M. *Phys. Chem. Chem. Phys.* **2010**, *12*, 5084.

(13) Small, D.; Zaitsev, V.; Jung, Y.; Rosokha, S. V.; Head-Gordon, M.; Kochi, J. K. *J. Am. Chem. Soc.* **2004**, *126*, 13850.

(14) Zheng, S.; Lan, J.; Khan, S. I.; Rubin, Y. *J. Am. Chem. Soc.* **2003**, *125*, 5786.

(15) Small, D.; Rosokha, S. V.; Kochi, J. K.; Head-Gordon, M. *J. Phys. Chem. A* **2005**, *109*, 11261.

(16) Zaitsev, V.; Rosokha, S. V.; Head-Gordon, M.; Kochi, J. K. *J. Org. Chem.* **2006**, *71*, 520.

(17) Uchida, K.; Hirao, Y.; Kurata, H.; Kubo, T.; Hatano, S.; Inoue, K. *Chem. - Asian J.* **2014**, *9*, 1823.

(18) Mou, Z.; Uchida, K.; Kubo, T.; Kertesz, M. *J. Am. Chem. Soc.* **2014**, *136*, 18009.

(19) Mou, Z.; Kubo, T.; Kertesz, M. *Chem. - Eur. J.* **2015**, *21*, 18230.

(20) Goto, K.; Kubo, T.; Yamamoto, K.; Nakasuji, K.; Sato, K.; Shiomi, D.; Takui, T.; Kubota, M.; Kobayashi, T.; Yakusi, K.; Ouyang, J. *J. Am. Chem. Soc.* **1999**, *121*, 1619.

(21) Fukui, K.; Sato, K.; Shiomi, D.; Takui, T.; Itoh, K.; Gotoh, K.; Kubo, T.; Yamamoto, K.; Nakasuji, K.; Naito, A. *Synth. Met.* **1999**, *103*, 2257.

(22) Morita, Y.; Suzuki, S.; Fukui, K.; Nakazawa, S.; Kitagawa, H.; Kishida, H.; Okamoto, H.; Naito, A.; Sekine, A.; Ohashi, Y.; Shiro, M.; Sasaki, K.; Shiomi, D.; Sato, K.; Takui, T.; Nakasuji, K. *Nat. Mater.* **2008**, *7*, 48.

(23) Perrin, C. L.; Dwyer, T. J. *Chem. Rev.* **1990**, *90*, 935.

(24) Tok, O. L.; Gridnev, I. D.; Korobach, E. M.; Bubnov, Y. N. *Chem. Commun.* **2000**, 311.

(25) Bennett, M. J., Jr.; Cotton, F. A.; Davison, A.; Faller, J. W.; Lippard, S. J.; Morehouse, S. M. *J. Am. Chem. Soc.* **1966**, *88*, 4371.

(26) Bestari, K. T.; Boere, R. T.; Oakley, R. T. *J. Am. Chem. Soc.* **1989**, *111*, 1579.

(27) (a) Zhao, Y.; Schultz, N. E.; Truhlar, D. G. *J. Chem. Phys.* **2005**, *123*, 161103. (b) Zhao, Y.; Schultz, N. E.; Truhlar, D. G. *J. Chem. Theory Comput.* **2006**, *2*, 364.

(28) (a) Becke, A. D. *J. Chem. Phys.* **1993**, *98*, 5648. (b) Lee, C.; Yang, W.; Parr, R. G. *Phys. Rev. B: Condens. Matter Mater. Phys.* **1988**, *37*, 785.

(29) Frisch, M. J.; Trucks, G. W.; Schlegel, H. B.; Scuseria, G. E.; Robb, M. A.; Cheeseman, J. R.; Scalmani, G.; Barone, V.; Mennucci, B.; Petersson, G. A.; Nakatsuji, H.; Caricato, M.; Li, X.; Hratchian, H. P.; Izmaylov, A. F.; Bloino, J.; Zheng, G.; Sonnenberg, J. L.; Hada, M.; Ehara, M.; Toyota, K.; Fukuda, R.; Hasegawa, J.; Ishida, M.; Nakajima, T.; Honda, Y.; Kitao, O.; Nakai, H.; Vreven, T.; Montgomery, J. A., Jr.; Peralta, J. E.; Ogliaro, F.; Bearpark, M.; Heyd, J. J.; Brothers, E.; Kudin, K. N.; Staroverov, V. N.; Kobayashi, R.; Normand, J.; Raghavachari, K.; Rendell, A.; Burant, J. C.; Iyengar, S. S.; Tomasi, J.; Cossi, M.; Rega, N.; Millam, J. M.; Klene, M.; Knox, J. E.; Cross, J. B.; Bakken, V.;

DOI: 10.1021/jacs.6b01791
J. Am. Chem. Soc. 2016, 138, 4665−4672

Adamo, C.; Jaramillo, J.; Gomperts, R.; Stratmann, R. E.; Yazyev, O.; Austin, A. J.; Cammi, R.; Pomelli, C.; Ochterski, J. W.; Martin, R. L.; Morokuma, K.; Zakrzewski, V. G.; Voth, G. A.; Salvador, P.; Dannenberg, J. J.; Dapprich, S.; Daniels, A. D.; Farkas, Ö.; Foresman, J. B.; Ortiz, J. V.; Cioslowski, J.; Fox, D. J. *Gaussian 09*, revision D.01; Gaussian, Inc.: Wallingford, CT, 2009.

DOI: 10.1021/jacs.6b01791
J. Am. Chem. Soc. 2016, 138, 4665−4672